

RESEARCH

Open Access



The influence of different clay/sand ratios on the hygrothermal properties of earthen plasters in the Maijishan Grottoes

Shanshan Yao¹, Zengfeng Yan^{2*}, Bokai Xu³, Wenbei Bi⁴, Junjie Zhang², Hao Li², Junhui Qu⁵ and Songhao Zhang⁵

Abstract

Variations in temperature and moisture content in the earthen plasters of the Maijishan Grottoes can readily lead to mural deterioration. This study investigates the influence of two different clay/sand ratios on the hygrothermal properties of earthen plasters in the Maijishan Grottoes. Two distinct types of earthen plasters samples were created with different clay/sand ratios: one with a weight ratio of 30:70 and another with a weight ratio of 70:30. The hygrothermal properties of earthen plasters samples were examined, and the temperature and moisture content variations were evaluated based on measurement data of hygrothermal environment in three caves. The findings revealed that the influence of the clay/sand ratios on thermal properties was relatively minor compared to its effect on hygric properties. Lower clay/sand ratio resulted in decreased thermal conductivity and specific heat capacity of earthen plasters, leading to increased temperature fluctuation, but the difference is minor. Additionally, in high-humidity environments, the difference in moisture content variations between the two types is greater than in low-humidity environments as the relative humidity changes. This research holds significant implications for the preservation of murals in the Maijishan Grottoes while also providing fresh perspectives for the restoration of multi-layered mural structures.

Keywords Earthen plasters, Heritage preservation, Hygrothermal properties, Maijishan Grottoes, Simulation analysis

Introduction

The Maijishan Grottoes, located in Tianshui City, Gansu Province, are renowned as one of the four great grottoes in China. The Maijishan Grottoes have 221 caves from various dynasties, along with a large number of murals

and statues. The cultural, historical, and artistic significance of the cultural relics within the Maijishan Grottoes is exceptionally high. As shown in Fig. 1, the cliffs of Maijishan Grottoes are composed of glutenite rock, resulting in a naturally uneven surface after excavation. Consequently, it is necessary to first apply earthen plasters onto the cliff surface before painting on the surface of earthen plasters. Most of the statues are made of clay sculpture. A wooden framework is initially constructed and then bound with straw. Coarse plaster is applied over the straw to shape the sculpture. Lastly, the fine plaster mixed with hemp is applied over the coarse plaster layer to perform intricate carving.

Changes in the hygrothermal environment can readily lead to water and salt migration within the earthen plasters, subsequently causing damage to cultural artifacts. Figure 2 illustrates schematic diagram of the

*Correspondence:

Zengfeng Yan
yanzengfeng@xauat.edu.cn

¹ School of Architecture, Zhengzhou University, Zhengzhou 450001, China

² School of Architecture, Xi'an University of Architecture and Technology, Xi'an 710055, China

³ Maijishan Grottoes Art Research Institute, Dunhuang Academy, Tianshui 741020, China

⁴ School of Architecture, Chang'an University, Xi'an 710000, China

⁵ Institute of Building Environment and Energy, China Academy of Building Research Co., Ltd, Beijing 100013, China



© The Author(s) 2024. **Open Access** This article is licensed under a Creative Commons Attribution 4.0 International License, which permits use, sharing, adaptation, distribution and reproduction in any medium or format, as long as you give appropriate credit to the original author(s) and the source, provide a link to the Creative Commons licence, and indicate if changes were made. The images or other third party material in this article are included in the article's Creative Commons licence, unless indicated otherwise in a credit line to the material. If material is not included in the article's Creative Commons licence and your intended use is not permitted by statutory regulation or exceeds the permitted use, you will need to obtain permission directly from the copyright holder. To view a copy of this licence, visit <http://creativecommons.org/licenses/by/4.0/>. The Creative Commons Public Domain Dedication waiver (<http://creativecommons.org/publicdomain/zero/1.0/>) applies to the data made available in this article, unless otherwise stated in a credit line to the data.



Fig. 1 The earthen plasters in the Maijishan Grottoes

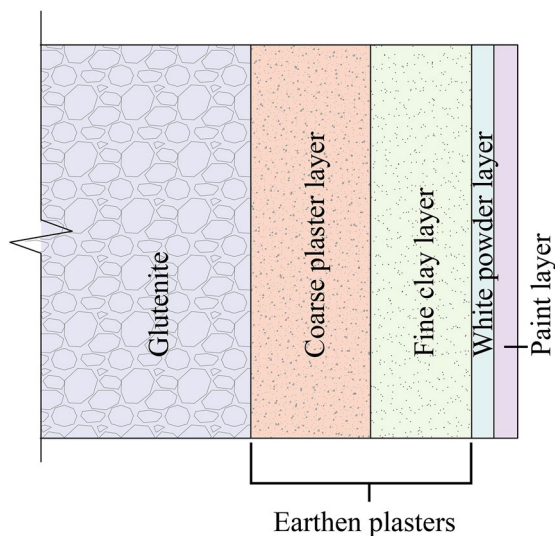


Fig. 2 Schematic diagram of the earthen plasters in the Maijishan Grottoes

earthen plasters in the Maijishan Grottoes. The murals in the Maijishan Grottoes primarily comprise a coarse plaster layer, a fine plaster layer, a white powder layer, and a paint layer. Collectively, the coarse plaster layer and fine plaster layer constitute the earthen plaster. Painted artifacts exhibit distinct layered structures, with each layer possessing unique thermal expansion and moisture expansion properties. As the hygrothermal environment changes, these differences can result in interlayer stresses within the mural, subsequently contributing to its degradation [1]. Additionally, under the influence of external environmental factors, epoxy resin may also undergo detachment from the earthen plasters [2]. The migration of capillary water can induce differential crystallization of insoluble salts, moderately soluble salts, and readily soluble salts within the

earthen plasters, consequently leading to salt damage in the murals [3]. The moisture in the air affects the capillary rise of the earthen plasters. Lower relative humidity leads to a greater migration of moisture to the air during capillary rise, while the salt accumulates in the lower part of the specimen [4]. The absorption of moisture by the earthen plasters can trigger the dissolution of soluble salts. Under high humidity conditions, NaCl can facilitate the deliquescence or hydration of other soluble salts, thus hastening the deterioration of murals [5]. External factors such as dustfall salt can expedite the water-salt transport in the earthen layer, ultimately causing damage to the statue [6]. Moreover, moisture can accelerate the reactions between compounds and the surrounding system, subsequently leading to the degradation of the paint film [7].

The composition of earthen plasters in different regions may not necessarily have the same proportions. Research conducted on the clay/sand ratios of earthen plasters in selected grottoes along the Silk Road revealed notable differences. For instance, in the Mogao Grottoes, earthen plasters predominantly consist of clay, with a content ranging from 50 to 80%. In the Tiantishan Grottoes, earthen plasters of murals contain around 70% to 80% clay content. However, in the Bingling Temple Grottoes, the majority of earthen plasters exhibits clay content of approximately 50% [8]. Changes in composition have a notable impact on the hygrothermal characteristics of the materials. The lime stabilized bentonite composite showed high specific surface area and isothermal vapor sorption capacity, surpassing the other five clay composites studied [9]. Incorporating plant fibers can effectively alter the properties of earthen plasters. For example, incorporating rice husk into caves plaster reduces cracking and improves durability, but it is also crucial to consider the antifungal, antibacterial, and insect resistant properties of plant fibers [10]. Straw, hemp, and corn cob

have been found to decrease the thermal conductivity of earth, with a slight increase in specific heat capacity, but decrease storage inertia [11]. Incorporating olive fibers into the earth matrix enhances both insulation and hygric properties [12]. Plaster samples with 2% corn pith exhibited a substantial 78% decrease in thermal conductivity, along with moderate improvements in water vapor permeability and moisture buffering capacity [13]. The novel bio-clay plaster, created by incorporating hemp powder into clay, displayed excellent moisture buffering capability and low thermal conductivity [14]. Furthermore, the clay/sand ratio also plays a role in performance of earthen plasters. Studies have shown that the addition of organic admixture and plant fibers increases the clay content of earthen plaster, enhancing its moisture buffering capacity [15]. Mehmet et al. [16] assessed how the clay/sand ratio affects the performance of clay plaster, revealing an optimal range of 0.43 to 0.66 (by weight) when considering both shrinkage and compressive strength results. Increasing plaster clay content improves bending strength, reinforcing the plaster, but it also results in increased shrinkage, potentially weakening the interface between the plaster and the wall [17].

The research of hygrothermal properties of cultural heritage materials is of paramount importance for the preservation of cultural artifacts. When combined with hygrothermal simulation model, it enables the investigation of various factors affecting the hygrothermal environment [18, 19]. In the field of architectural engineering, research on the hygrothermal properties of materials is quite extensive. These include investigations into novel integrated structures using various materials to enhance the building envelope's hygrothermal performance [20], the influence of factors such as fiber size and binders on the hygrothermal properties of natural insulation materials [21], the impact of different building materials on indoor hygrothermal environments [22], and the effects of moisture content on the hygrothermal parameters of building materials [23]. In the field of heritage conservation, understanding the effects of air-conditioning operation is vital to safeguard the structure and building materials from fluctuations in outdoor hygrothermal load [24]. For historical Chinese blue bricks, Li et al. [25] conducted measurements of the equilibrium moisture content across different relative humidity conditions and found that blue bricks exhibited higher moisture absorption capabilities compared to modern blue and clay bricks. Franzen et al. [26] conducted static equilibrium sorption measurements on six building stones to retrieve correlations between material characteristics essential for weathering processes. The thermal fatigue test on sandstone and mortar used in heritage buildings have demonstrated that variations in thermal expansions and thermal

stresses can result in the separation of the stone-mortar interface [27]. Non-destructive methods for moisture testing in historical buildings, such as the microwave method and the dielectric method, have been discussed by Hola [28]. Additionally, Litti et al. [29] utilized iterative passive infrared thermography and environmental monitoring to evaluate brick masonry hygrothermal behavior, revealing that thermal transmittance values in moist regions were over three times higher than in dry areas.

The research was conducted to investigate the influence of hygrothermal properties on the preservation of cultural artifacts. Taking into consideration the characteristics of earthen plasters in Maijishan Grottoes, two types of earthen plasters with different clay/sand ratios were prepared to analyze the impact of clay/sand ratios on the hygrothermal parameters of earthen plasters. Furthermore, by utilizing measured temperature and relative humidity inside the caves, a coupled hygrothermal transfer model was employed to compare the effects of different clay/sand ratios on the hygrothermal parameters of earthen plasters under varying hygrothermal environments. This study provides a quantitative analysis of the influence of clay/sand ratios on the hygrothermal properties of the murals, providing research methods for the conservation of cultural relics in the Maijishan Grottoes.

Experimental testing

Materials

The earthen plasters from the fragments of Maijishan Grottoes were analyzed. The coarse plaster of earthen plasters is relatively thick, with a thickness ranging from approximately 0.3 cm to 3 cm. The surface of the glutenite becomes uneven after excavation and the coarse plaster is directly applied to the glutenite surface. So to improve bonding, fibers are often added to the plaster. During the Later Qin to Song dynasties, wheat straw was commonly used as a fiber material in the coarse plaster layer, while hemp fibers were used during the Ming dynasty. The fine plaster layer is relatively thin, with a thickness of around 0.1 cm to 1 cm. In some fine plaster layers, hemp was added as fiber material, while in others, cotton and hemp fabric were added. The purpose of the white powder layer is to serve as a painting surface, with a thickness of approximately 0.01 cm. The earthen plaster in Maijishan Grottoes exhibit a relatively high sand content. The clay content ranges from 26 to 42%, with the majority around 30%, while the sand content ranges from 58 to 78%, predominantly around 70% [8]. Therefore, compared to other grottoes, the Maijishan Grottoes possess a higher sand content in their earthen plasters.

In comparison to the clay/sand ratios observed in the fragments of the caves, the earthen plasters utilized

for the restoration and reinforcement of the Maijishan Grottoes exhibit a clay/sand ratio of approximately 2:1 (by weight) [30], signifying a higher proportion of clay content. The restoration process involves using locally sourced clay, which undergo clay desalting treatment. Wheat straw is commonly added to the coarse plaster, while hemp is incorporated into the fine plaster. Prior to application, the hemp, known to contain impurities and microorganisms, undergoes sun-drying and beating, followed by soaking in purified water and subsequent drying. Wheat straw and hemp are typically cut into lengths of 1–2 cm using scissors.

Sample preparation

Considering the difference in clay/sand ratios of earthen plasters between fragments and the materials used for restoration, a research was conducted to compare the impact of clay/sand ratios on the hygrothermal properties of earthen plasters. Two types of earthen plaster samples with different clay/sand ratios were prepared using locally materials for testing and analysis (Fig. 3).

The earthen plaster consists of a coarse plaster layer and a fine plaster layer. Table 1 presents two types of earthen plaster, denoted as Type A and Type B. Each type includes both the coarse and the fine plaster layer, with wheat straw added to the coarse plaster layer and hemp added to the fine plaster layer. The research aims to compare the hygrothermal properties of the two types of earthen plaster, considering the influence of wheat straw and hemp in each type. As shown in Table 1, the clay/sand weight ratio of the earthen plaster in Type A samples is 30:70, and in Type B samples is 70:30. The testing methods for density, porosity, thermal conductivity, isothermal moisture absorption, and water vapor permeability were adopted from previous studies conducted by the research group [31]. The method for thermal diffusivity testing involves raising the sample to a specific



Fig. 3 Raw materials for earthen plasters samples

Table 1 Compositions of earthen plaster samples

Notation	Composition	Composition			
		Clay (w%)	Sand (w%)	Wheat straw (w%)	Hemp (w%)
Type A	Coarse plaster	30	70	2	–
	Fine plaster	30	70	–	2
Type B	Coarse plaster	70	30	2	–
	Fine plaster	70	30	–	2

temperature and allowing it to reach a uniform and stable state, then calculating its thermal diffusivity value based on the cooling rate at a stable cooling temperature. The testing procedure adheres to reference standards [32]. The method for permeability testing involves measuring the flow rate through the sample over a certain period and then calculating the material’s permeability. The testing procedure follows the reference standards [33].

Test results

Density and porosity

Referencing relevant literature [34, 35], the mercury intrusion method was employed to conduct porosity test on the earthen plaster samples. In the mercury intrusion method, the pore diameter range is between 4 nm and 360 μm. Testing through other methods has shown that pores within this diameter range constitute the majority of the pore diameter distribution for these types of samples. Therefore, the results measured by the mercury intrusion method were used for analysis.

As presented in Table 2, the test results for Type A and Type B are quite similar, albeit with slight variations. The true density of Type A closely approximates that of Type B. True density refers to the mass of solid particles per unit volume in a compact state and apparent density is the ratio of the mass of a material to its apparent volume. Specifically, Type A exhibits an apparent density of 1610.25 kg/m³ with a porosity of 27.11%, while Type B has an apparent density of 1519.71 kg/m³ with a porosity of 30.18%. It is worth noting that in the dry state, sand has a higher density compared to clay. Type A has a higher sand content and a

Table 2 Results of porosity and density

	Type A	Type B
Porosity (%)	27.11	30.18
Ture Density (kg/m ³)	2209.15	2176.61
Apparent density (kg/m ³)	1610.25	1519.71

lower porosity compared to Type B, resulting in a higher apparent density for Type A than for Type B.

Figure 4a depicts the relationship between the cumulative mercury intrusion and intrusion pressure. As the intrusion pressure gradually increases, the cumulative mercury intrusion decreases. At a pressure of 33,000 psia, Type A exhibits a cumulative mercury intrusion of 0.148 ml/g, while Type B shows a higher value of 0.172 ml/g. In Fig. 4b, the relationship between mercury intrusion pore size diameter and cumulative mercury intrusion is presented. For mercury intrusion pore size diameters ranging from 100 nm to 14,000 nm, Type A displays a larger cumulative mercury intrusion than Type B, indicating that within this range of pore size diameters, Type A has a higher porosity than Type B. However, for pore size diameters smaller than 100 nm and larger than 14000 nm, cumulative mercury intrusion of Type A is smaller than that of Type B, suggesting that within this range of pore size diameters, Type A has a lower porosity than Type B. Nevertheless, from the cumulative mercury intrusion of pore size diameters, it can be observed that Type B has a higher porosity than Type A.

Thermal conductivity and specific heat capacity

Table 3 presents the test results for the thermal conductivity, thermal diffusivity, and specific heat capacity of the dried samples at 25 °C. The specific heat capacity is calculated using the following formula:

$$\alpha = \frac{\lambda}{\rho c} \tag{1}$$

where α is the thermal diffusivity, m^2/s ; λ is the thermal conductivity, $W/m\cdot k$; ρ is the density, kg/m^3 ; c is the specific heat capacity, $J/kg\cdot K$.

Table 3 The thermal conductivity, thermal diffusivity and specific heat capacity of samples

	Type A	Type B
Thermal conductivity (W/m·k)	0.215	0.275
Thermal diffusivity (m^2/s)	1.66×10^{-7}	1.78×10^{-7}
Specific heat capacity (J/kg·K)	806	1013

The thermal conductivity of Type A sample is 0.215 W/m·k, while Type B sample exhibits a thermal conductivity of 0.275 W/m·k. Dry sand has a thermal conductivity of 0.22 W/m·k [36], and dry soil has a thermal conductivity of 0.58 W/m·k [37]. Both Type A and Type B samples have lower thermal conductivities than dry soil, primarily due to the inclusion of plant fibers in the samples. The plant fibers reduce the density of the samples, while enhancing their insulation properties. The specific heat capacity of soil minerals ranges from 711.5 to 1088.1 J/kg·K [38]. The specific heat capacities of both Type A and Type B samples fall within this range. Notably, Type A sample exhibits lower thermal conductivity, thermal diffusivity, and specific heat capacity compared to Type B sample. This difference can be ascribed to the increased sand content in Type A, leading to a slight decrease in the thermal performance of the sample in completely dry conditions.

Water vapor permeability

The water vapor permeability coefficient was tested using the dry–wet cup method, and the results are presented in Table 4. Under the same humidity conditions, Type A exhibits a smaller water vapor permeability coefficient than Type B. In low humidity environments, the

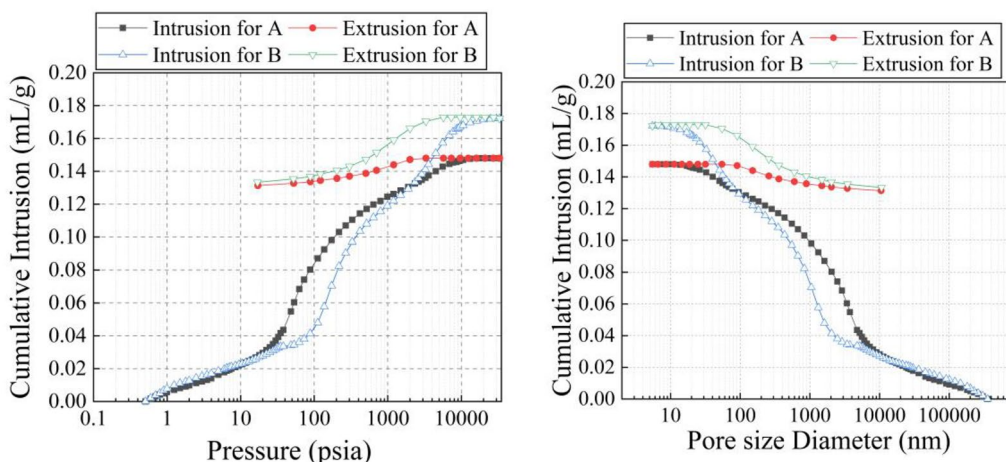


Fig. 4 a Cumulative mercury intrusion–distribution curve of mercury intrusion pressure. b Cumulative mercury intrusion–pore diameter distribution curve

Table 4 Water vapor permeability

Notation	Relative humidity inside the cup	Relative humidity outside the cup (%)	Relative humidity difference (%)	Water vapor permeability kg/(m·s·Pa)	Water vapor resistance factor
Type A	0	54.4	54.4	1.68×10^{-11}	11.86
	54.4%	84.3	29.9	0.78×10^{-11}	25.59
	84.3%	97.3	13	7.2×10^{-11}	2.76
Type B	0	54.4	54.4	1.77×10^{-11}	11.39
	54.4%	84.3	29.9	1.13×10^{-11}	17.73
	84.3%	97.3	13	9.2×10^{-11}	2.14

Table 5 Relative humidity of air corresponding to different saturated salt solutions at 25 °C [39]

Name	Molecular formula	Relative humidity (%)
Lithium chloride	LiCl	11.3 ± 0.3
Magnesium chloride	MgCl ₂	32.8 ± 0.2
Potassium carbonate	K ₂ CO ₃	43.2 ± 0.4
Magnesium nitrate	Mg(NO ₃) ₂	52.9 ± 0.2
Sodium chloride	NaCl	75.3 ± 0.1
Potassium chloride	KCl	84.3 ± 0.3
Potassium nitrate	KNO ₃	93.6 ± 0.6
Potassium sulfate	K ₂ SO ₄	97.3 ± 0.5

water vapor permeability coefficients of both Type A and Type B samples are relatively close. However, in medium to high humidity environments, the difference in water vapor permeability coefficient between Type A and Type B increases, indicating that Type B shows better water vapor permeability in such conditions. In the Dunhuang Mogao Grottoes, the earthen plaster composed of clay, sand, and hemp with a weight ratio of 64:36:3 has a water vapor permeability coefficient of 1.15×10^{-11} kg/(m·s·Pa) [31]. This value is similar to the water vapor permeability coefficient of Type B in medium to low humidity conditions. The difference can be attributed to variations in material composition and the geographical origin of the materials. In high humidity conditions, there is a significant increase in the vapor permeability coefficient, indicating that the earthen plaster exhibits enhanced moisture permeability in high-humidity environments.

Sorption isotherms

Through fitting the relative humidity and equilibrium moisture content of the material at a certain temperature, the material’s sorption isotherms can be derived. The experiment utilized eight types of saturated salt solutions. As shown in Table 5, the corresponding air

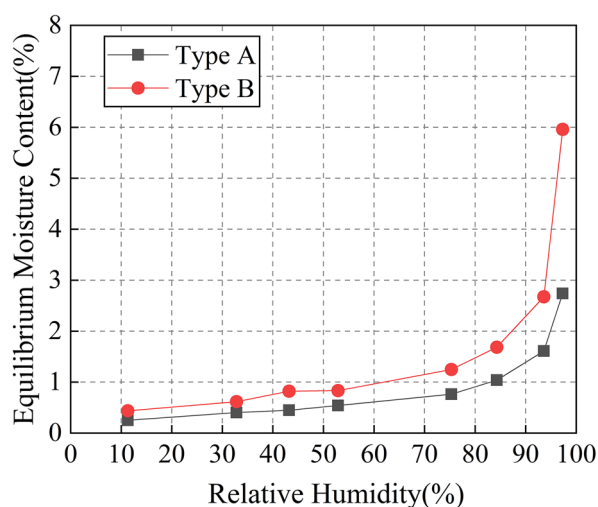


Fig. 5 Test results of equilibrium moisture content of the samples

relative humidity for the saturated salt solutions are 11.3%, 32.8%, 43.2%, 52.9%, 75.3%, 84.3%, 93.6%, and 97.3%.

Figure 5 illustrates the test results of the equilibrium moisture content for the two types of samples. The results show that within the relative humidity range of 11.3 to 97.3%, the equilibrium moisture content of Type A varies from 0.25 to 2.74%, while Type B ranges from 0.44 to 5.96%. Relevant literature indicates that as the clay content increases, the moisture content of the earthen plasters increases under the same relative humidity [40, 41]. So the equilibrium moisture content of Type B are higher than that of Type A. Both types demonstrate a slower rate of increase in equilibrium moisture content at relative humidity levels below 75.3%. However, the rate of increase accelerates when the relative humidity exceeds 75.3%.

The test results were fitted using several models, which included the BET model (Eq. 2) [42], the GAB model (Eq. 3) [43], the Peleg model (Eq. 4) [44], and the Kumaran model (Eq. 5) [45]. The formulations are as follows:

$$w(\varphi) = \frac{a\varphi}{(1 + b\varphi)(1 - c\varphi)} \tag{2}$$

$$w(\varphi) = \frac{abc\varphi}{(1 - b\varphi)(1 - b\varphi + bc\varphi)} \tag{3}$$

$$w(\varphi) = a\varphi^b + c\varphi^d \tag{4}$$

$$w(\varphi) = \frac{\varphi}{a\varphi^2 + b\varphi + c} \tag{5}$$

The fitting results are presented in Fig. 6, and the constants obtained from the fitting are listed in Table 6. The Adjusted R² values for all four models are greater than 0.960, indicating a highly accurate fit to the data. For the two types of earthen plaster samples, the Peleg model demonstrates the highest fitting accuracy, with an Adjusted R² of 0.990 for Type A and 0.992 for Type B. The fitting results reveal that both Type A and Type B adsorption curves follow an S-shaped pattern, consistent with Type II isotherm of the IUPAC standard [46]. These

materials possess both macroporous and mesoporous characteristics. The moisture content at saturation is close to 3% for Type A and approximately 6% for Type B. Overall, at the same relative humidity levels, the equilibrium moisture content in Type B is 1.5 to 2.1 times higher than that in Type A. Earthen plasters with a higher clay content demonstrate a greater capacity for moisture absorption and retention.

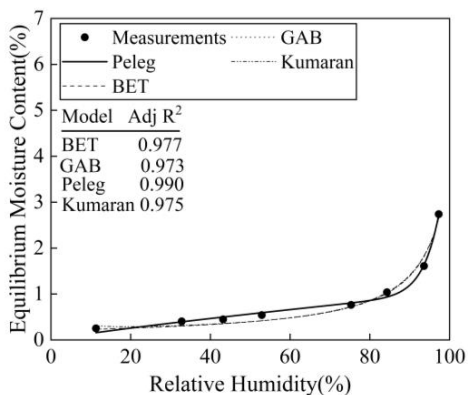
Permeability

Permeability refers to the ability of a material to allow fluid to pass through under a certain pressure difference. The formula for calculating permeability is as follows [47]:

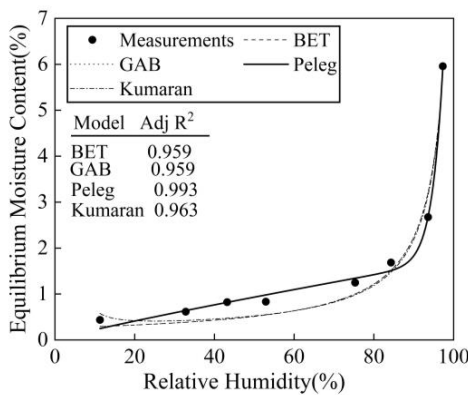
$$K = k \frac{g}{\nu} \tag{6}$$

where K is the permeability coefficient, cm/s; k is the permeability, m²; g is the acceleration of gravity, m/s²; ν is the kinematic viscosity coefficient of water, m²/s.

Table 7 presents the test results for the permeability coefficient of the samples and the corresponding



(a) Type A



(b) Type B

Fig. 6 Sorption isotherms of samples

Table 6 Specific function expressions and error

Model	Sample	Constants	Adj R ²
BET model	Type A	a = 12, b = 5.765 × 10 ³ , c = 0.947	0.977
	Type B	a = 12, b = 4.602 × 10 ³ , c = 0.982	0.966
GAB model	Type A	a = 2.09 × 10 ⁻³ , b = 0.946, c = 1.181 × 10 ⁴⁵	0.973
	Type B	a = 2.62 × 10 ⁻³ , b = 0.982, c = -1.268 × 10 ⁴⁵	0.959
Peleg model	Type A	a = 1.023 × 10 ⁻² , b = 0.855, c = 3.384 × 10 ⁻² , d = 24.460	0.990
	Type B	a = 0.114, b = 35.981, c = 0.0173, d = 0.892	0.993
Kumaran model	Type A	a = -486.788, b = 528.989, c = -17.158	0.975
	Type B	a = -422.319, b = 455.331, c = -26.545	0.963

Table 7 Permeability coefficient and permeability of samples

	Type A	Type B
Permeability coefficient (cm/s)	1.401×10^{-5}	3.791×10^{-6}
Permeability (m^2)	1.434×10^{-14}	3.88×10^{-15}

permeability. The test results clearly indicate that Type A has higher values for both the permeability coefficient and permeability compared to Type B, suggesting that Type A exhibits a greater ability to allow moisture penetration. According to the literature, the permeability coefficient of silty clay ranges from 1×10^{-6} to 1×10^{-5} cm/s, while for sand, it is between 1×10^{-3} and 1×10^{-1} cm/s [48]. As Type A contains more sand, it exhibits a higher permeability coefficient, which aligns with the predicted results. Additionally, this implies that under conditions of higher moisture content, Type A demonstrates a stronger capability for moisture penetration.

Methodology

To further investigate the impact of different clay/sand ratios on the temperature and moisture content of the earthen plasters, a hygrothermal transfer analysis model was developed for the cave wall. Three distinct types of measured hygrothermal environments inside the caves were employed as boundary conditions to quantitatively assess the influence of clay/sand ratios on the temperature and moisture content of the earthen plasters.

Simulation model

The hygrothermal transfer analysis model for the cave wall was established using the Moist Porous Media Module of the COMSOL Multiphysics software. COMSOL Multiphysics software is widely utilized for simulating hygrothermal transfer in materials [49–51]. The one-dimensional model, depicted in Fig. 7, consists of a cliff thickness of 15m and an earthen plaster thickness of

0.035m. The left boundary conditions, as shown in the figure, have a constant temperature of 12.2 °C [19], and a relative humidity of 100%. On the right side, there is convective heat and mass exchange between the wall surface and the air in the cave, with the temperature and relative humidity taken from field measurements in the cave. The upper and lower interfaces are considered adiabatic and impermeable to moisture; that is, the heat and moisture transfer rate is 0. Point 1 is the analysis point for the simulated results of temperature and moisture content in the earthen plasters. The mesh of the model near the earthen plaster is denser, while it becomes sparser away from the earthen plaster. The maximum growth rate of mesh elements is 1.1, and the total number of elements is 131. The model employs a transient solution method with a time step of 1 h. The solver is PARDISO, and the model is solved using the backward difference formula method.

Environmental parameters

Three representative and diverse types of caves in the Majijishan Grottoes were selected for conducting measurements of the hygrothermal environment near the walls, in order to obtain the boundary conditions on the right side of the model in Fig. 7. The selected caves include Cave 101, Cave 127, and Cave 25 (Fig. 8). Cave 25 is open and shallow, highly susceptible to external climate influences. Cave 127 has a greater depth with a relatively small ventilation opening, while Cave 101 features a smaller depth and ventilation opening. The monitoring period was from 1:00 on January 16, 2019 to 24:00 on December 31, 2019, with measurements taken at hourly intervals. The HOBO U23-001 data logger was utilized as the monitoring instrument, offering a temperature range of -40 to 70 °C and a relative humidity range of 0% to 100%. The temperature accuracy is ± 0.18 °C, and the relative humidity accuracy is $\pm 2.5\%$.

The measured results, illustrated in Fig. 9, reveal that Cave 25 exhibits temperature and relative humidity

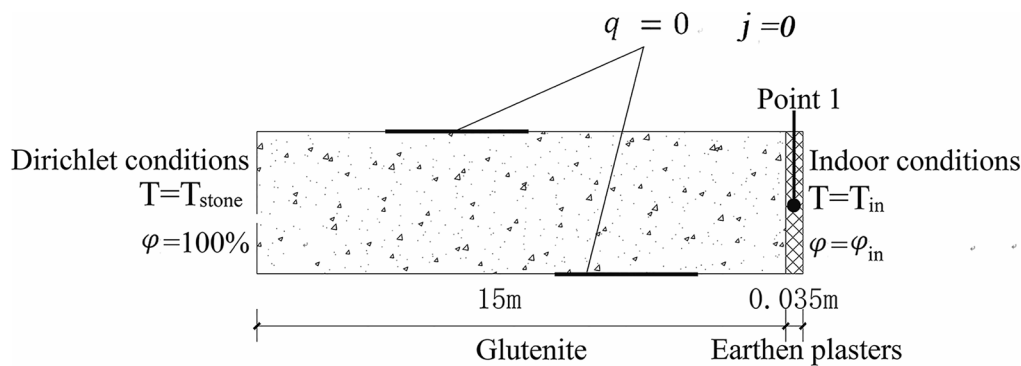


Fig. 7 Schematic diagram of the hygrothermal transfer analysis model

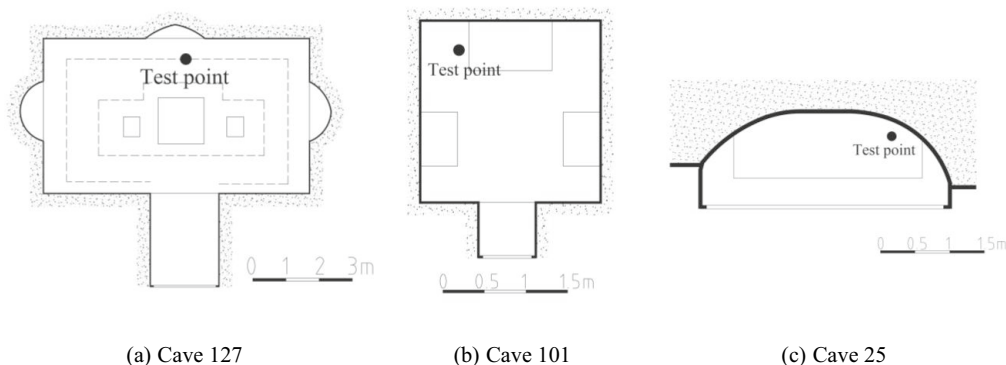


Fig. 8 The layout diagrams of the three caves

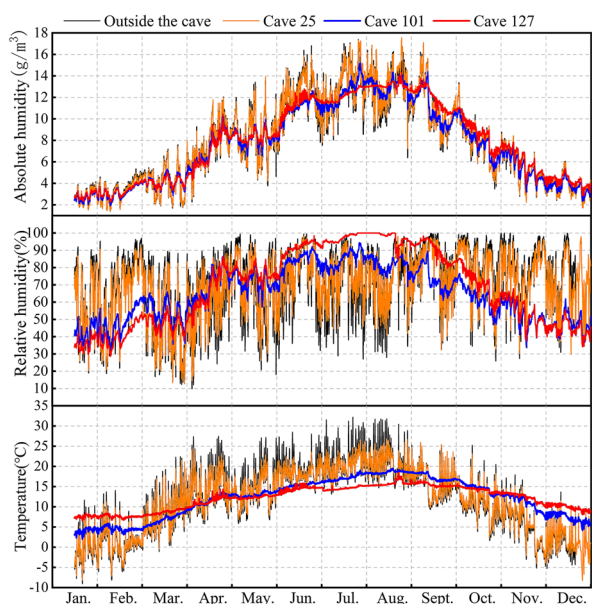


Fig. 9 Measured results of temperatures, relative humidity, and absolute humidity in three caves

values inside the cave similar to the external environment, attributed to its larger cave door and ventilation area. The lowest temperature throughout the year is -8.3°C , while the highest temperature reaches 26.8°C .

The relative humidity shows no significant overall trend throughout the year, with the monthly average values ranging from 52.2 to 79.6%. Additionally, the absolute humidity fluctuates from 1.4 to 17.6 g/m^3 over the year. Both Cave 101 and Cave 127 display distinct seasonal variations, with lower temperature and relative humidity during winter and higher temperature and relative humidity during summer. For the monthly average values, Cave 101 experiences an annual temperature fluctuation of 14.5°C , a relative humidity fluctuation of 41.7%, and an absolute humidity fluctuation of 10.3 g/m^3 . In contrast, Cave 127 exhibits a smaller annual temperature fluctuation of 8.1°C , a larger relative humidity fluctuation of 61.7%, and a similar absolute humidity fluctuation of 10.2 g/m^3 . Moreover, during summer, Cave 127 experiences a prolonged period of relative humidity staying at 100%.

Simulation settings

The model was set up using the Moist Porous Media module in the Comsol Multiphysics software. Neglecting the changes in heat and moisture caused by natural convection within the medium, the wind speed value is set to 0 m/s. The hygrothermal properties of glutenite were referenced from Table 8. The dry density, porosity, and isothermal sorption curve were measured in the laboratory. The permeability coefficient, thermal conductivity,

Table 8 Hygrothermal properties of glutenite

Parameters	Dry density	Porosity	Dry specific heat	Dry thermal conductivity	Permeability coefficient	The absorption isotherm	
Unit	kg/m^3	-	$\text{J}/(\text{kg}\cdot\text{K})$	$\text{W}/(\text{m}\cdot\text{K})$	cm/s	The model	Fitting parameter
Glutenite	2449.62	0.072	860	2.28	6.0×10^{-6}	$u = k_1 \phi^{k_2} + k_3 \phi^{k_4}$	$k_1 = 5.74 \times 10^{-3}$ $k_2 = 0.207$ $k_3 = 5.78 \times 10^{-3}$ $k_4 = 6.691$

and specific heat were obtained from references [52–54]. The convective heat transfer coefficient was set at 8.7 W/(m²·K) [55], and the convective mass transfer coefficient was calculated using Formula 7 [56]. The initial values for the earthen plaster and the adjacent 0.5m of glutenite were set at a temperature of 6°C and a relative humidity of 80%. The remaining part was initialized with a temperature of 8°C and a relative humidity of 95%. The simulation interval was set at 1 h.

$$h_m = \frac{D_v}{\lambda} \left(\frac{\lambda}{\rho c D_v} \right)^n h_c \tag{7}$$

where h_m is convection mass transfer coefficient (m/s); D_v is vapor diffusivity in air (m²/s); λ is thermal conductivity, W/m·K; ρ is density, kg/m³; c is specific heat capacity, J/(kg·K); h_c is convection heat transfer coefficient, W/(m²·K); n is the analogical factor exponent, $n = 1/3$.

Simulation results

Figure 10 illustrates the simulation results of temperature and moisture content in earthen plasters of the three

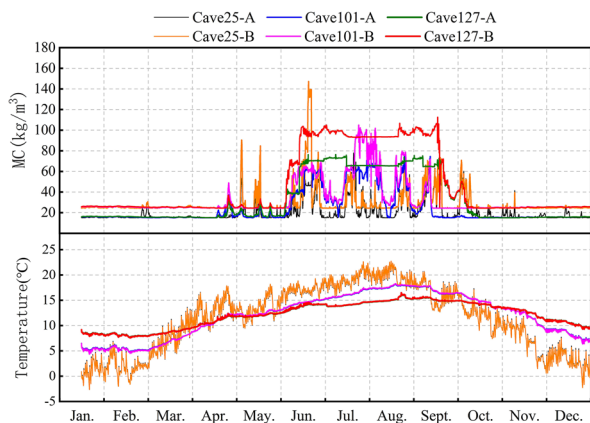


Fig. 10 Simulated results of temperature and moisture content in earthen plasters of three caves

caves. The observed trend reveals lower temperature and moisture content during winter, whereas higher temperature and moisture content during summer. Within the same cave, the temperature difference in earthen plasters between Type A and Type B is negligible, while the moisture content in Type A is lower than in Type B. Comparing the three caves, the annual temperature difference of the monthly average values in the earthen plaster follows this order: Cave 127 < Cave 101 < Cave 25. Conversely, the annual moisture content difference of the monthly average values follows this order: Cave 127 > Cave 101 > Cave 25.

The statistical results of the monthly average temperature and moisture content are presented in Table 9. The highest monthly average temperature occurs in August or September, while the lowest monthly average temperature occurs in January or February. Within the same cave, the difference in monthly average temperature of earthen plasters between Type A and Type B is minimal. Among the three caves, the highest monthly average temperature follows this order: Cave 25 > Cave 101 > Cave 127, with a difference of approximately 4.7°C between Cave 25 and Cave 127. Conversely, the lowest monthly average temperature follows this order: Cave 25 < Cave 101 < Cave 127, with a difference of 6.8°C between Cave 25 and Cave 127. Regarding the monthly average moisture content of earthen plasters, there is a significant difference between Type A and Type B. Among the three caves, the highest monthly average moisture content in Type B is 15.6 kg/m³ higher than Type A in Cave 25, 11.6 kg/m³ higher in Cave 101, and 27.0 kg/m³ higher in Cave 127. For the lowest monthly average moisture content, Type B is 9.4 kg/m³ higher than Type A in Cave 25, 9.3 kg/m³ higher in Cave 101, and 9.6 kg/m³ higher in Cave 127. The variation pattern shows that for months with lower absolute humidity inside the caves, the difference in monthly average moisture content between Type B and Type A in three caves is relatively close. However, for months with high absolute humidity, Cave 127 with the

Table 9 The annual maximum and minimum values of monthly average temperature and moisture content

		Cave25-A	Cave25-B	Cave101-A	Cave101-B	Cave127-A	Cave127-B
Maximum monthly average temperature	Values (°C)	19.8	19.9	17.6	17.7	15.2	15.2
	Month	August	August	August	August	September	September
Minimum monthly average temperature	Values (°C)	1.3	1.2	5.3	5.3	8.1	8.0
	Month	January	January	February	February	February	February
Maximum monthly average moisture content	Values(kg/m ³)	30.1	45.6	46.6	58.1	69.4	96.4
	Month	September	June	July	July	July	July
Minimum monthly average moisture content	Values(kg/m ³)	15.4	24.8	15.3	24.7	15.3	24.9
	Month	January	April	March	October	November	November

highest relative humidity exhibits the largest difference in monthly average moisture content between the two types of earthen plasters.

Discussion and analysis

Due to the variations in temperature and moisture of earthen plasters, murals can be susceptible to damage. In order to compare the stability of temperature and moisture content in earthen plasters, a comparative analysis is conducted using the indicators as follows:

$$\Delta m = m_i - m_{i-1} \tag{8}$$

where Δm is the variation; m_i is the value at time i ; m_{i-1} is the value at time $i-1$.

Figure 11 shows the statistical analysis of the variation in temperature and moisture content of earthen plasters for the three caves. From the graph, it can be seen that, in most cases, the absolute values ΔT for the three caves is slightly higher for Type A compared to Type B, with minimal difference between them. At the same time, Cave 101 and Cave 127 exhibit relatively smaller ΔT values, while Cave 25 shows a relatively larger ΔT . Regarding ΔMC , there is a noticeable seasonal variation trend, with significant fluctuations observed from June to September. Based on the field measurements, it is noted that during the period from June to September, the absolute humidity inside the caves are relatively high. In high relative humidity conditions, the equilibrium moisture content of earthen plasters changes more rapidly. Consequently, when examining the annual variation trend, ΔMC values are higher in the months of June to September compared to other months.

In order to further analyze the monthly cumulative changes in temperature and moisture content of earthen plasters, statistical analysis is performed using MCI

(Monthly Cumulative Increment) and MCR (Monthly Cumulative Reduction). The formulas are as follows:

$$\begin{cases} MCR = \sum_{i=1}^n (m_i - m_{i-1}), m_i - m_{i-1} < 0 \\ MCI = \sum_{i=1}^n (m_i - m_{i-1}), m_i - m_{i-1} \geq 0 \end{cases} \tag{9}$$

MCI is derived by summing up the positive values of Δm for each month, whereas MCR is obtained by summing up the negative values of Δm for each month. MCR and MCI enable a more straightforward comparison of the variations in temperature and moisture content for each month. Importantly, the MCR values are negative, and a smaller negative value indicates a larger cumulative reduction in that particular month.

The statistical results are shown in Fig. 12. From Fig. 12a–c, it can be observed that there are slight differences in the MCR and MCI values of temperature between the two types of earthen plasters in three caves, with Type A having slightly higher absolute values compared to Type B. The maximum MCI values of temperature for the entire year are as follows: 95.3 °C for Type A and 89.0 °C for Type B in Cave 25, 11.6 °C for Type A and 10.8 °C for Type B in Cave 101, and 9.1 °C for Type A and 8.4 °C for Type B in Cave 127. On the other hand, the minimum MCR values of temperature for the entire year are as follows: -86.6 °C for Type A and -80.2 °C for Type B in Cave 25, -13.7 °C for Type A and -12.9 °C for Type B in Cave 101, and -8.6 °C for Type A and -8.1 °C for Type B in Cave 127. There is no apparent pattern in the MCR and MCI variation of temperature from the annual trend perspective. The larger absolute values of Cave 25 compared to the other two caves can be attributed to the larger air temperature fluctuations within the Cave 25, while Cave 101 and Cave 127 exhibit relatively smaller air temperature variations. Considering the test results of thermal properties, the thermal conductivity of Type A and Type B in earthen plasters are close, while the specific heat of Type A is slightly lower than Type B. Thus, under similar environmental conditions, the monthly cumulative variations of temperature is slightly higher for Type A compared to Type B.

Based on Fig. 12d–f, the annual variation trend shows that both types of earthen plasters in three caves exhibit a pattern of low moisture content in winter and high moisture content in summer. In the Cave 25, Type A has a greater monthly cumulative variations in moisture content than Type B for most months, with the largest difference between the two types in MCI being 148.1 kg/m³, and in MCR being 148.2 kg/m³. In the Cave 101, the difference in MCI between Type B and Type A is significant for July and August, with a maximum value of 256.4 kg/m³. Similarly, in the Cave 127, the difference in MCI

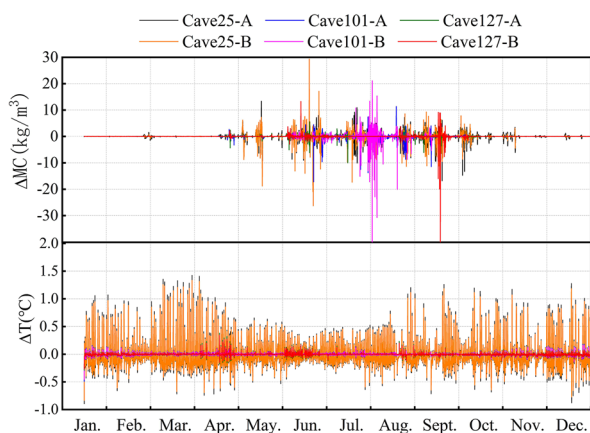


Fig. 11 Hourly variations in temperature and moisture content of earthen plasters in three caves

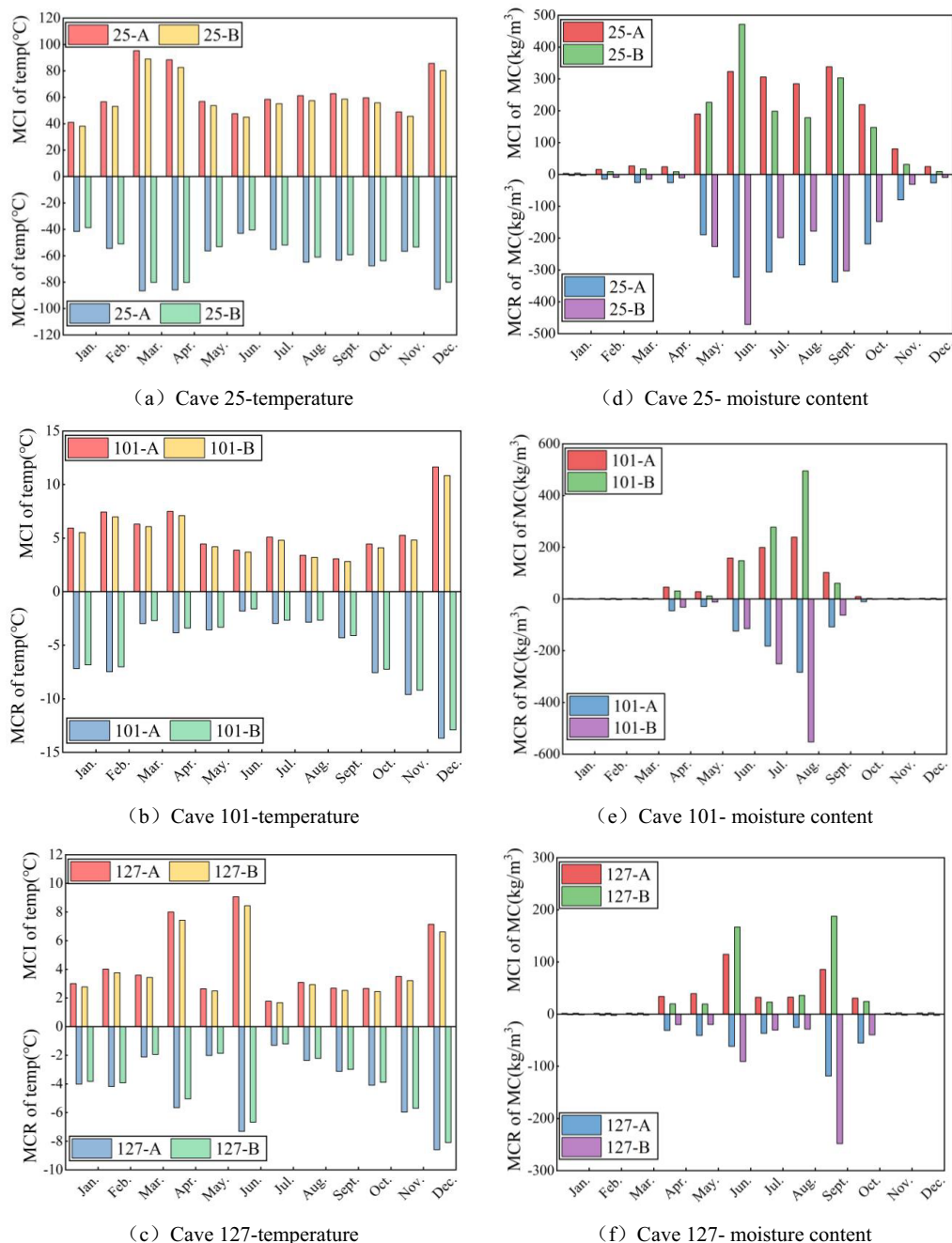


Fig. 12 Monthly accumulated variations in temperature and moisture content of earthen plasters

between the two types is significant for June and September, with a maximum value of 102.1 kg/m³. Based on the hygric properties test results, Type A has smaller water vapor permeability and equilibrium moisture content than Type B. However, in high relative humidity environments, the water vapor permeability and equilibrium moisture content increase significantly. This indicates that in months with higher relative humidity, the monthly

cumulative variations in moisture content is higher compared to other months.

Based on the analysis results, it is evident that the clay/sand ratios significantly influence the hygrothermal properties of earthen plasters, consequently impacting the annual variations in temperature and moisture content. A higher sand content leads to a relatively smaller thermal conductivity and specific heat capacity of earthen

plasters, resulting in a minor increase in temperature variation under the same environmental conditions. However, this impact on temperature is relatively small due to the minimal difference. In contrast, the influence of clay/sand ratios on the moisture content of earthen plasters is more pronounced. A higher sand content leads to a relatively lower moisture content. During months with significant fluctuations in relative humidity, the clay/sand ratios exhibit a more noticeable effect on the variation in moisture content under high humidity conditions. Increasing the sand content in earthen plasters can effectively reduce the changes in moisture content associated with fluctuations in relative humidity under high humidity conditions. However, it is essential to consider that a substantial increase in sand content may affect the adhesion between the earthen plaster and the wall surface. Therefore, further research is required to analyze the clay/sand ratios from the perspective of stress to better understand its implications for repairing the earthen plasters.

Conclusion

Because the clay/sand ratios of earthen plasters for cave remnants and restoration is different in the Maijishan Grottoes, two types samples of earthen plasters were prepared using locally available materials. Subsequently, hygrothermal properties tests were conducted on both samples types. Finally, based on measurements of the internal hygrothermal environment in three caves, the variations in temperature and moisture content of the two types were assessed under different cave conditions. The following conclusions were drawn from the research:

1. The clay/sand ratio has a smaller influence on thermal properties compared to hygric properties. The thermal conductivity of two types is relatively similar, but samples with higher sand content exhibit relatively lower specific heat capacity and thermal diffusivity. The vapor permeability coefficient and equilibrium moisture content are relatively higher in samples with lower sand content, and this difference increases under high humidity conditions compared to samples with higher sand content. The permeability of samples with higher sand content is also relatively higher.
2. The clay/sand ratio has a limited impact on the temperature variation of earthen plasters. Higher sand content leads to a relatively smaller thermal conductivity and specific heat capacity, resulting in a slight increase in temperature variation under the same environmental conditions, but the difference is minor.

3. The clay/sand ratio significantly affects the variation in moisture content of earthen plasters. Under high humidity conditions, the difference in moisture content between the two types becomes more significant, making earthen plasters more susceptible to drastic changes in moisture content.

The study conducted experimental testing and simulation analyses on samples of earthen plasters with two different clay/sand ratios. Although the clay/sand ratio has a minor impact on the temperature in earthen plasters, it significantly influences the moisture content. Therefore, in future research, the study can further investigate the effects of different clay/sand ratios on earthen plasters of the Maijishan Grottoes, taking into account the characteristics of stress variations. This research provides new insights into the degradation and restoration of multi-layered murals.

Abbreviations

c	Specific heat capacity (J/kg·K)
D_v	Vapor diffusivity in air (m^2/s)
g	Acceleration of gravity (m/s^2)
h_c	Convection heat transfer coefficient ($W/(m^2\cdot K)$)
h_m	Convection mass transfer coefficient (m/s)
K	Permeability coefficient (cm/s)
k	Permeability (m^2)
MCR	Monthly cumulative reduction
MC	Moisture content (kg/m^3)
MCI	Monthly cumulative increment
ΔMC	Variation of moisture content (kg/m^3)
ΔT	Variation of temperature ($^{\circ}C$)
α	Thermal diffusivity (m^2/s)
λ	Thermal conductivity ($W/m\cdot K$)
ρ	Density (kg/m^3)
Υ	Kinematic viscosity coefficient of water (m^2/s)
φ	Relative humidity (%)

Acknowledgements

Not applicable.

Author contributions

SY and ZY conducted the experiments, analyzed the data and wrote the paper. BX and HL conducted the field measurements of the caves. WB and JZ analyzed the data. JQ and SZ conducted the testing of samples. All authors reviewed the manuscript.

Funding

This project was supported by the National Natural Science Foundation of China (Project No. 52208037, No. 51978554, No.52278127 and No. 52308085) and Project of Gansu Cultural Relics Bureau (No. GSWW202223).

Availability of data and materials

The datasets used and/or analyzed during the current study are available from the corresponding author on reasonable request.

Declarations

Ethics approval and consent to participate

Not applicable.

Competing interests

The authors declare that they have no competing interests.

Received: 6 October 2023 Accepted: 17 January 2024
Published online: 25 January 2024

References

- He X, Xu M, Zhang H, Zhang B, Su B. An exploratory study of the deterioration mechanism of ancient wall-paintings based on thermal and moisture expansion property analysis. *J Archaeol Sci*. 2014;42:194–200.
- Li Q. Analysis on the causes of cracks disease on mural paintings of Yuan dynasty in Fengguo temple. Xi'an: Northwest university; 2019.
- Yan L. Salt efflorescence in earth plaster generated by unsaturated water migration. Lanzhou: Lanzhou University; 2009.
- Jiang X, Zhang H, Yan G, Wang J. Research on effects of humidity on capillary migration of salt solutions in mural plaster. *Rock Soil Mech*. 2014; 459–65.
- Li F, Wang X, Guo Q, Zhang B, Pei Q, Yang S. Moisture adsorption mechanism of earthen plaster containing soluble salts in the Mogao Grottoes of China. *Stud Conserv*. 2018;64:159–73.
- Qiu L, Qiao J, Ma L, Yang Y. Research on the effect of the Dustfall on the statue surface on the water migration of the earthen layer. *IOP Conf Ser Earth Environ Sci*. 2021;632: 022020.
- Issa YM, Abdel-Maksoud G, Ibrahim M, Magdy M. A combination of analytical methods to evaluate the effect of humidity aging on the painting materials of icon models. *Vib Spectrosc*. 2020;107: 103010.
- Li Z. Conservation of the wall paintings and colored statures of the grottoes on the silk road. Beijing: Science press; 2005.
- Liuzzi S, Hall MR, Stefanizzi P, Casey SP. Hygrothermal behaviour and relative humidity buffering of unfired and hydrated lime-stabilised clay composites in a Mediterranean climate. *Build Environ*. 2013;61:82–92.
- Dighe B, Singh MR, Pokharia AK. Ancient Indian techniques for sustainable and environmentally friendly decorative earthen plasters of Karla and Bhaja Caves. *India Mater Today Proc*. 2020;32:536–43.
- Laborel-Préneron A, Magniont C, Aubert J-E. Hygrothermal properties of unfired earth bricks: effect of barley straw, hemp shiv and corn cob addition. *Energy Build*. 2018;178:265–78.
- Liuzzi S, Rubino C, Stefanizzi P, Petrella A, Boghetich A, Casavola C, et al. Hygrothermal properties of clayey plasters with olive fibers. *Constr Build Mater*. 2018;158:24–32.
- Palumbo M, McGregor F, Heath A, Walker P. The influence of two crop by-products on the hygrothermal properties of earth plasters. *Build Environ*. 2016;105:245–52.
- Jiang Y, Phelipot-Mardele A, Collet F, Lanos C, Lemke M, Ansell M, et al. Moisture buffer, fire resistance and insulation potential of novel bio-clay plaster. *Constr Build Mater*. 2020;244: 118353.
- Lagouin M, Laborel-Préneron A, Magniont C, Geoffroy S, Aubert J-E. Moisture buffer capacity of a bilayer bio- and geo-based wall. *Constr Build Mater*. 2022;329: 127209.
- Emiroğlu M, Yalama A, Erdoğdu Y. Performance of ready-mixed clay plasters produced with different clay/sand ratios. *Appl Clay Sci*. 2015;115:221–9.
- Hamard E, Morel J-C, Salgado F, Marcom A, Meunier N. A procedure to assess the suitability of plaster to protect vernacular earthen architecture. *J Cult Herit*. 2013;14:109–15.
- Bi W, Yan Z, Zhang Z, Yao S, Zhang J, Wang X. Modeling and numerical simulation of heat and mass transfer in the cave wall of the Mogao Grottoes in China. *Build Environ*. 2021;201: 108003.
- Yao S, Yan Z, Ma Q, Xu B, Zhang Z, Bi W, et al. Analysis of the annual hygrothermal environment in the Maijishan Grottoes by field measurements and numerical simulations. *Build Environ*. 2022;221: 109229.
- Wu D, Rahim M, El Ganaoui M, Bennacer R, Djedjig R, Liu B. Dynamic hygrothermal behavior and energy performance analysis of a novel multilayer building envelope based on PCM and hemp concrete. *Constr Build Mater*. 2022;341: 127739.
- Zhou Y, Trabelsi A, El Mankibi M. Hygrothermal properties of insulation materials from rice straw and natural binders for buildings. *Constr Build Mater*. 2023;372: 130770.
- Damle RM, Khatri N, Rawal R. Experimental investigation on hygrothermal behaviour of cement and lime plaster. *Build Environ*. 2022;217: 109098.
- Abbas MS, McGregor F, Fabbri A, Ferroukhi MY, Perlot C. Effect of moisture content on hygrothermal properties: comparison between pith and hemp shiv composites and other construction materials. *Constr Build Mater*. 2022;340: 127731.
- Chae Y, Kim SH. Selection of retrofit measures for reasonable energy and hygrothermal performances of modern heritage building under dry cold and hot humid climate: a case of modern heritage school in Korea. *Case Stud Therm Eng*. 2022;36: 102243.
- Li Y, Ma Y, Xie H, Li J, Li X. Cross validation of hygrothermal properties of historical Chinese blue bricks with isothermal sorption experiments. *Front Archit Res*. 2021;10:164–75.
- Franzen C, Mirwald PW. Moisture content of natural stone: static and dynamic equilibrium with atmospheric humidity. *Env Geol*. 2004. <https://doi.org/10.1007/s00254-004-1040-1>.
- Morillas H, Vazquez P, Maguregui M, Marcaida I, Silva LFO. Composition and porosity study of original and restoration materials included in a coastal historical construction. *Constr Build Mater*. 2018;178:384–92.
- Hola A. Measuring of the moisture content in brick walls of historical buildings—the overview of methods. *IOP Conf Ser: Mater Sci Eng*. 2017;251: 012067.
- Litti G, Koshdel S, Audenaert A, Braet J. Hygrothermal performance evaluation of traditional brick masonry in historic buildings. *Energy Build*. 2015;105:393–411.
- Ou X, Zhang R. Survey and Analysis of the disease to mud sculptures and murals in Cave 72 of the Maijishan Grottoes. Proceedings of the 12th National Conference on Archaeology and Cultural Heritage Conservation Chemistry. 2012. pp. 306–310.
- Bi W, Yan Z, Zhao H, Sun L, Wang X, Zhang Z. The influence of two natural reinforcement fibers on the hygrothermal properties of Earthen plasters in Mogao Grottoes of China. *J renew mater*. 2020;8:1691–710.
- Technical requirements of the materials for external thermal insulation composite systems based on cellular glass. *JG/T 469–2015*; 2015.
- Standard for geotechnical testing method. *GB/T 50123–2019*; 2019.
- Lima J, Faria P, Santos SA. Earth plasters: the influence of clay mineralogy in the plasters' properties. *Int J Archit Heritage*. 2020;14:948–63.
- García-Vera VE, Tenza-Abril AJ, Lanzón M. The effectiveness of ethyl silicate as consolidating and protective coating to extend the durability of earthen plasters. *Constr Build Mater*. 2020;236: 117445.
- Sui X, Yu M, Peng X. Experimental study on thermal conductivity measurement of wet sands. *J Thermal Sci Technol*. 2009; 20–24.
- Liu D, Zhao H, Liu X, He Q. Thermal conductivity test of adobe materials with different moisture content and its effect on building energy consumption. *J Civil Environ Eng*. 2017; 20–25.
- Shao M, Wang Q, Huang H. *Soil Physics*. Beijing: Higher Education Press; 2006.
- Hygrothermal performance of building materials and products—Determination of hygroscopic sorption properties. *GB/T 20312–2006/ISO 12571:2000*; 2006.
- Chen C, Ren T, Hu K, Li B, Wang Y. Estimation of soil clay content using hygroscopic water content at an arbitrary humidity. *Soil Sci Soc Am J*. 2014;78:119–24.
- Arthur E, Tuller M, Moldrup P, Jensen DK, De Jonge LW. Prediction of clay content from water vapour sorption isotherms considering hysteresis and soil organic matter content. *Eur J Soil Sci*. 2014;66:206–17.
- Anderson RB. Modifications of the Brunauer, Emmett and Teller equation 1. *J Am Chem Soc*. 1946;68:686–91.
- van den Berg C, Bruin S. Water activity and its estimation in food systems: theoretical aspects. Amsterdam: Elsevier; 1981. p. 1–61.
- Peleg M. Assessment of a semi-empirical four parameter general model for sigmoid moisture sorption isotherms. *J Food Process Eng*. 1993;16:21–37.
- Kumaran KM. Heat, air and moisture transport in envelope parts. Paris: Laboratorium Bouwfysica; 1996.
- Sing KSW. Reporting physisorption data for gas/solid systems with special reference to the determination of surface area and porosity (Recommendations 1984). *Pure Appl Chem*. 1985;57:603–19.
- Yin Z. Principles of geotechnical engineering. Beijing: China Water & Power Press; 2007.
- Zhao M, Wang Y. *Soil mechanics and foundation engineering*. Wuhan: Wuhan University of Technology Press; 2014.
- Promis G, Douzane O, Le Tran AD, Langlet T. Moisture hysteresis influence on mass transfer through bio-based building materials in dynamic state. *Energy Build*. 2018;166:450–9.

50. Huang P, Chew YMJ, Chang W-S, Ansell MP, Lawrence M, Latif E, et al. Heat and moisture transfer behaviour in *Phyllostachys edulis* (Moso bamboo) based panels. *Constr Build Mater*. 2018;166:35–49.
51. Kupczak A, Sadłowska-Sałęga A, Krzemień L, Sobczyk J, Radoń J, Kozłowski R. Impact of paper and wooden collections on humidity stability and energy consumption in museums and libraries. *Energy Build*. 2018;158:77–85.
52. Yang T. Study on technology of permeation and humid prevention of Majijishan Grottoes. Master Thesis. Lanzhou University, Lanzhou; 2011.
53. Yu R, Huang S, Zhang J, Xu W, Ke T, Zuo Y, et al. Measurement and analysis of the thermal conductivities of rock samples from the Baiyinchagan Sag and Uliastai Sag, Erlian Basin, northern China. *Acta petrologica sinica*. 2020;36:621–36.
54. Liu Y, Tang H. *Rock mechanics*. Beijing: China university of geosciences press; 1999.
55. Liu X. *Building physics*. 3rd ed. Beijing: China architecture & building press; 2010.
56. Incropera FP, Dewitt DP. *Fundamentals of heat and mass transfer*. Hoboken: John Wiley & Sons; 2006.

Publisher's Note

Springer Nature remains neutral with regard to jurisdictional claims in published maps and institutional affiliations.